KEK Preprint 2004-86
February 2005
H

Undoped-CsI Calorimeter for the $K_L^0 \to \pi^0\nu\bar{\nu}$ Experiment at KEK-PS

M. Doroshenko[a], K. Abe[b], J.K. Ahn[c], Y. Akune[b], V. Baranov[d], Y. Fujioka[b], Y.B. Hsiung[e], T. Ikei[f], T. Inagaki[a,g], S. Ishibashi[b], H. Ishii[f], T. Iwata[l], S. Kobayashi[b], S. Komatsu[f] T.K. Komatsubara[g], A. Kurilin[d], E. Kuzmin[d], A. Lednev[h], H.S. Lee[c], S.Y. Lee[c], G.Y. Lim [g],T. Matsumura[i], T. Mizuhashi[f], A. Moisseenko[d], T. Morimoto[g], T. Nakano[j], N. Nishi[f], J. Nix[h], T. Nomura[k], T. Oba[f], H. Okuno[g], K. Omata[g], G.N. Perdue[h], S. Perov[d], S. Podolsky[d], S. Porokhovoy[d], K. Sakashita[f], N. Sasao[k], H. Sato[l], T. Sato[g], M. Sekimoto[g], T. Shinkawa[i], Y. Sugaya[f], A. Sugiyama[b], T. Sumida[j], Y. Tajima[l], Z. Tsamalaidze[d], T. Tsukamoto[b], Y. Wah[h], H. Watanabe[h], M. Yamaga[f], T. Yamanaka[f], H.Y. Yoshida[l] and Y. Yoshimura[g]

[a] *Dept. of Particle and Nuclear physics, School of High Energy Accelaror Science, The Graduate Univ. for Advanced Science (SOKENDAI), Tsukuba, Ibaraki, 305-0801, Japan*

[b] *Dept. of Physics, Saga Univ., Saga 840-8502, Japan*

[c] *Dept. of Physics, Pusan National Univ., Busan, 609-735, Republic of Korea*

[d] *Joint Institute for Nuclear Research, 141980 Dubna, Moscow Region, Russian Federation*

[e] *Dept. of Physics, National Taiwan Univ,. Taipei, 10617, The Republic of China*

[f] *Dept. of Physics, Osaka Univ., Toyonaka, Osaka, 560-0043, Japan*

[g] *High Energy Accelerator Research Organization (KEK), Tsukuba, Ibaraki, 305-0801, Japan*

[h] *Enrico Fermi Institute, Univ. of Chicago, Chicago, IL 60637, U.S.A.*

[i] *National Defense Academy, Yokosuka, Kanagawa 239-8686, Japan*

[j] *Research Center for Nuclear Physics. Osaka Univ., Ibaraki, Osaka, 567-0047, Japan*

[k] *Dept. of Physics, Kyoto Univ,. Kyoto, 606-8502, Japan*

[l] *Dept. of Physics, Yamagata Univ,. Yamagata, 990-8560, Japan*

Submitted to Nucl. Instrm. Method Phys. Research A

High Energy Accelerator Reserch Organization

High Energy Accelerator Research Organization (KEK), 2005

KEK Reports are available from:

Science Information and Library Services Division
High Energy Accelerator Research Organization (KEK)
1-1 Oho, Tsukuba-shi
Ibaraki-ken, 305-0801
JAPAN

Phone: +81-29-864-5137
Fax: +81-29-864-4604
E-mail: irdpub@mail.kek.jp
Internet: http://www.kek.jp

Undoped CsI calorimeter

for the $K_L^0 \to \pi^0 \nu\bar{\nu}$ experiment at KEK-PS

M. Doroshenko[a], K. Abe[b], J.K. Ahn[c], Y. Akune[b], V. Baranov[d], Y. Fujioka[b], Y.B. Hsiung[e], T. Ikei[f], T. Inagaki,[a,g,*], S. Ishibashi[b], H. Ishii[f], T. Iwata[l], S. Kobayashi[b], S. Komatsu[f], T. K. Komatsubara[g], A. Kurilin[d], E. Kuzmin[d], A. Lednev[h], H.S. Lee[c], S.Y. Lee[c], G.Y. Lim[g], T. Matsumura[i], T. Mizuhashi[f], A. Moisseenko[d], T. Morimoto[g], T. Nakano[j], N.Nishi[f], J. Nix[h], T. Nomura[k], T. Oba[f], H.Okuno[g], K. Omata[g], G.N. Perdue[h], S. Perov[d], S. Podolsky[d], S. Porokhovoy[d], K. Sakashita[f], N. Sasao[k], H. Sato[l], T. Sato[g], M. Sekimoto[g], T. Shinkawa[i], Y. Sugaya[f], A.Sugiyama[b], T. Sumida[j], Y. Tajima[l], Z. Tsamalaidze[d],T. Tsukamoto[b], Y. Wah[h], H. Watanabe[h], M. Yamaga[f], T. Yamanaka[f], H.Y. Yoshida[l] and Y. Yoshimura[g]

[a] *Dept. of Particle and Nuclear Physics, School of High Energy Accelerator Science, The Graduate Univ. for Advanced Science (SOKENDAI), Tsukuba, Ibaraki, 305-0801, Japan*

[b] *Dept. of Physics, Saga Univ., Saga, 840-8502, Japan*

[c] *Dept. of Physics, Pusan National Univ., Busan, 609-735, Republic of Korea*

[d] *Joint Institute for Nuclear Research, 141980 Dubna, Moscow Region, Russian Federation*

[e] *Dept. of Physics, National Taiwan Univ., Taipei, 10617, The Republic of China*

[f] *Dept. of Physics, Osaka Univ., Toyonaka, Osaka, 560-0043, Japan*

[g] *High Energy Accelerator Research Organization (KEK), Tsukuba, Ibaraki, 305-0801, Japan*

[h] *Enrico Fermi Institute, Univ. of Chicago, Chicago, IL 60637, U.S.A.*

[i] *National Defense Academy, Yokosuka, Kanagawa, 239-8686, Japan*

[j] *Research Center for Nuclear Physics, Osaka Univ., Ibaraki, Osaka, 567-0047, Japan*

[k] *Dept. of Physics, Kyoto Univ., Kyoto, 606-8502, Japan*

[l] *Dept. of Physics, Yamagata Univ., Yamagata, 990-8560, Japan*

(To be submitted to Nucl. Instr. & Meth. in Physics Research A)

Abstract

An electromagnetic calorimeter consisting of 576 undoped CsI crystals has been used to search for the $K_L^0 \to \pi^0 \nu \bar{\nu}$ decay at the KEK 12-GeV proton synchrotron (E391a). The calorimeter is placed in a vacuum of lower than 10^{-1} Pa. Special energy and timing calibrations have been performed. The energy calibration started from a check of the linearity for nine sample crystals using an electron beam. Then, after mounting all crystals in the E391a detector, we made an in situ calibration of the energy by using cosmic ray and punch-through muons. The gain constants obtained from both muons agree with each other with an accuracy of 2.3% (σ). They were further refined by using $\gamma\gamma$ samples from π^0's produced off an aluminum plate (5-mm thick) hit by neutral beam particles. Using the final gain constants, we obtained a K_L^0 mass resolution of 4.3 MeV/c^2 (σ) for the $K_L^0 \to \pi^0 \pi^0 \pi^0$ decay. Also, using the timing constants measured for cosmic rays, we obtained a resolution of 0.51 ns (σ) for the timing difference among six γ's in the $K_L^0 \to \pi^0 \pi^0 \pi^0$ decay.

Keywords: CsI calorimeter; Energy calibration; Timing calibration; K_L^0 decay

PACS code: 29.40

* Corresponding author: Tel.: +81-29-864-5413; fax: +81-29-864-7831 .

E-mail address: inagaki@post.kek.jp

1. Introduction

The E391a experiment is proposed to search for the rare kaon decay, $K_L^0 \rightarrow \pi^0 \nu\bar{\nu}$, at the KEK 12-GeV proton synchrotron [1]. This decay mode originates from a direct CP-violation process. Measurements of this branching ratio will provide us an important phase parameter, η, of the CKM mass matrix [2]. The branching ratio expected by the Standard Model is 3×10^{-11}, and the present experimental upper limit is 5.9×10^{-7}, measured by the KTeV group [3]. E391a, having a sensitivity of 3×10^{-10}, is a first step for further experimental studies at J-PARC [4].

The experimental setup is shown in Fig. 1. Two γ's decaying from π^0 are detected by an undoped CsI crystal calorimeter. Surrounding the CsI calorimeter, photon and charged-particle veto detectors are arranged in a cylindrical shape in order to reject backgrounds from other K_L^0 decays, like $K_L^0 \rightarrow \pi^0\pi^0\pi^0$ and $K_L^0 \rightarrow \pi^0\pi^0$. High detection efficiencies of these detectors are crucial for background rejection. These are arranged so as to tightly cover the fiducial K_L^0 decay region, and are placed in a vacuum to minimize any dead material in front of them.

Since the CsI calorimeter measures two γ's positively, precise energy and position determination of γ is important to identify the $K_L^0 \rightarrow \pi^0 \nu\bar{\nu}$ decay. In addition, a precise hit-timing measurement is mandatory to reject accidental hits in the CsI calorimeter. An undoped CsI crystal, which has a moderate light output and a fast time response, is one of the best materials to meet these requirements.

In this case it is crucial to make a good calibration within a few % in energy and sub nanosecond in timing [5]. We carried out these calibrations in multi-steps. After checking the operation of all CsI modules in a vacuum, sample tests for 9 modules were made by using electron beams in the energy range of 0.5-3.0 GeV. The good linearity found in the test confirmed that the

energy response can be expressed by a single parameter of the gain factor to a good approximation. After mounting CsI crystals in the experimental area we made an in situ calibration of the energy and hit timing by using cosmic ray and punch-through muons. Refinements of these gain constants were made by using the π^0 production data from the aluminum target in a special run.

In this report we mainly describe these calibration procedures of the CsI calorimeter and the obtained results.

2. CsI calorimeters

2-1 Setup

The arrangement of the CsI crystals in a support cylinder is shown in Fig. 2. Surrounding the neutral beam of 6 cm in diameter a collar counter (CC03), which is made of tungsten and scintillator plates, is placed. Next, 24 CsI modules of 5 x 5 x 50 cm^3 [6] are arranged. Since these crystals are borrowed from the KTeV group we call them KTeV CsI. After these, 496 CsI crystals of size 7 x 7 x 30 cm^3 (main CsI) [7] are stacked. At the periphery of the cylinder 56 CsI modules of a trapezoidal shape and 24 modules of a lead-scintillator sandwich fill the gap. These modules are stacked with a space of less than 100 μm between each other by applying pressure from both the horizontal and vertical directions. A photograph of the CsI stacking process is shown in Fig. 3.

2-2 Undoped CsI calorimeter module

Schematic drawings of two types of CsI modules, the main CsI and the KTeV CsI, are shown in Fig. 4.

Since these modules are operated in a vacuum we modified the HV divider so as to (1) reduce any heat dissipation and to (2) reduce heat conduction from the divider to the PMT and CsI crystal. For (1) we decreased

the divider current. For (2) we took a longer space between the PMT tube and the PC board on which resisters are mounted. The PC board is contained in a 2 mm thick aluminum cylinder and the inside space is filled with heat-conductive glue (METACAST 5448 [8]) which is 5-mm thick. The aluminum cylinder is connected thermally to the cooling water pipe.

The electric discharge in a vacuum depends on the arrangement of the HV terminals in the PMT divider. We measured the pressure dependence of the discharge voltage for several PMT's. The typical result is shown in Fig. 5, where the HV trip voltage is shown as a function of the vacuum pressure.

A vacuum pressure of less than 1 Pa is required for a safe operation of the PMT's.

2-3 Cooling system

Most of the heat is generated at the PMT voltage divider. It is only 0.6W for each PMT, but it reaches 300W in total. In a vacuum the heat can not be removed by convection but is transferred to the vacuum vessel through the PMT and crystals by conduction if there is no special cooling system. This results in two problems.

One is a high-temperature problem at the divider and the PMT. In the case of no special cooling, temperatures at the divider, the PMT and the crystal increase to a temperature higher than the room temperature in an equilibrium stage. Especially for the modules in the central part of the cylinder, near to the beam hole, the divider and the PMT become hot with 50^{o}C and 30^{o}C above the room temperature, respectively. This might cause problems for the safe operation of the PMT and cause a local increase of the vacuum pressure inside the divider due to a higher rate of outgassing.

The other problem is an inhomogeneity of temperature within a single crystal. Since the light output from an undoped CsI crystal depends largely on the temperature such a local variation of the temperature might cause several problems concerning the linearity and resolution.

In order to avoid these problems, we used a water-cooling

configuration, as shown in Fig. 6. Temperature-controlled water is circulated through copper pipes of 8mm diameter. Eight parallel lines are placed just behind the PMT divider and each line covers about 70 PMT's. A copper-braided flat cable, which is usually used for the ground line in electronics, connects the PMT divider and the copper pipe. The cable rounds the aluminum cylinder containing the PMT divider.

By watching the temperatures at the front and rear faces of several crystals, we optimized the water temperature to be 10 ^{o}C lower than the room temperature. We could keep the fluctuation of the PMT and the crystal temperatures within 0.2 ^{o}C during the whole running time for 5-months from February to June by setting the room and water temperatures to be 20 ^{o}C and 10 ^{o}C, respectively. Such an extremely good stability is a benefit of a setup where large detectors are placed in a vacuum.

2-4 Electronics and DAQ system

In the E391a experiment the signal from each CsI crystal is used for three purposes: (1) for an energy measurement, (2) for a hit-timing measurement and (3) for triggering. For signal splitting we have developed a so-called Amp-Discri module, shown in Fig. 7.

The module accepts 16 PMT signals from the front panel and provides (1) 16 through signals, (2) 16 discriminator outputs and (3) 2 outputs of 8-channel linear sum signals. The circuit parts are assembled in a double-span NIM package. In order to prevent any deterioration of the timing due to distortion of the signal shape, Amp-Discri modules are placed close to the detector, outside of the vacuum vessel. The noise level of the electronics system is minimized by careful grounding and shielding of the detectors, electronics circuits and cables. The effective threshold for a timing measurement can be lowered down to 0.5 mV. During data taking we set the threshold to be 1 mV, which corresponds to an energy of 1 MeV.

The linear-sum signals were used for event triggers, which we call "cluster triggers". The pattern to bundle eight CsI blocks for a sum signal is

shown in Fig. 8. Seventy-two clusters are formed and the cluster signals after discrimination were sent to the trigger logic. An event trigger was generated based on the number of hit clusters, N. The threshold of the cluster energy was set to be 40-100 MeV, depending on the type of triggers.

A schematic drawing of the DAQ system of the E391a experiment is shown in Fig. 9 [9]. Three output signals from the Amp-Discri module are sent to the DAQ system through coaxial cables (analogue signal) and twisted pair cables (digital signals). Timing and energy signals are delayed by about 300 ns relative to the linear-sum signal at the counting hut. These cables were placed in a box-type cable tray made of 2 mm-thick steel plates whose inner surfaces were covered by 200 μm-thick copper foil.

For the energy measurement, we used LeCroy 1885F FASTBUS ADC's [10], which have a 15 bit (50fC/bit) resolution and 96 input channels. The ADC covers the full range with two modes, high gain (0.05 pC/ch) and low gain (0.4 pC/ch) mode. The pedestal widths for all CsI modules are less than 1.5 ch (high gain) and 1.0 ch (low gain).

For the timing measurement we used TKO-TDC with a 200 ns full range and 50 ps resolution [11]. The threshold for the TDC signal was set at 1 mV, which corresponded to a deposited energy of 1 MeV in CsI. Since the analogue sum of 8 CsI blocks is used for triggering we adjusted the timing in front of the Amp-Discri module within a few nano seconds by trimming cables between the PMT and the Amp-Discri module. The DAQ system runs under the basic scheme of MIDAS [12].

3. CsI test before assembling

3-1 Sample calibration with the electron beam

Before assembling crystals into the support cylinder we performed a beam test using a momentum-analyzed electron beam in the momentum range between 0.5 GeV and 3.0 GeV at the $\pi 2$ beam line of the KEK 12-GeV proton synchrotron. The main purpose of this test was to check the response linearity. The momentum range of the beam was chosen so that the maximum energy of γ measured in E391a would be 2 GeV.

Twenty-five CsI modules and beam trigger counters are arranged as shown in Fig. 10. The inner nine modules are the modules to be calibrated because they are placed under the same surrounding conditions. Copper plates with water cooling surround the 5 x 5 stack to stabilize the temperature.

An electron beam was injected to the central position of each of nine modules. The beam profile was defined to be 10 mm x 10 mm by S3. The momentum of the beam was reexamined and corrected by a TOF measurement of protons and deuterons between S1 and S5, where the distance between two counters was 13 m and the CsI calorimeter was removed from the beam line during the TOF measurement. The corrections to the nominal momentum values were within few % for each set. The momentum spread was adjusted by an upstream collimator to be $\pm$1%. The particle species was identified by TOF and with a pair of gas Cherenkov counters, GC1 and GC2.

We studied the relation between the deposited energy and the output charge measured by a charge-sensitive ADC. The deposited energy was calculated by using of the GEANT3 simulation code, where the exact geometry of the calorimeter was taken into account. About 85% of the energy was deposited in the center crystal and about 15% escaped to the neighboring

crystals, or backward. These values slightly varied with the incident electron energy.

Figure 11 shows the relation between the peak values of the deposited energy and the output charge distributions measured by ADC for the inner 9 modules. The peak values were obtained by fitting the distributions with a Gaussian function.

The deviation of the experimental data from a linear fit is shown in Fig. 12. No significant or systematic deviation was observed among all nine modules and the maximum deviation was 2%. It was thus concluded that the conversion from the ADC channel number ($ADC(i)$) to the deposited energy ($E(i)$) for an i-th crystal can be obtained by a single gain constant ($g(i)$) as

$$E(i) = g(i) \cdot ADC(i) , \qquad (1)$$

within 2% accuracy, where $ADC(i)$ is the value after pedestal subtraction.

3-2 Test of all modules in a vacuum

Before stacking CsI crystals in the support cylinder, all modules were examined during their operation in a vacuum by using cosmic rays. It was necessary to check the response and to select good modules, because these crystals were recycles that had been fabricated more than 10 years ago.

We set the criteria to obtain an output gain of 2.4 pC/MeV in which the applied voltage should be in a range from 1.2 kV to 1.6 kV. In the test we measured the outputs of each module at 5 points in the longitudinal direction, and also set the criteria that the non-uniformity would not exceed 20%. Several modules exceeded these criteria; we did not use these.

4. CsI calibration after assembling

4-1 Calibration with cosmic rays

After assembling all CsI modules in the support cylinder we made an in situ calibration using cosmic rays. The calibration was performed regularly at any stage of the experiment, as well as a punch-through muon calibration (described in the next section).

For a cosmic-ray trigger we used the same trigger scheme as that for the physics run. We requested at least four cluster hits having a deposited energy of above 40 MeV.

The cosmic-ray trajectory was obtained from fitting the CsI hit pattern by a straight line, event by event. We requested at least 10 hits along the track. Figure 13 shows a typical event display.

The path length across a single crystal was calculated by using the trajectory and the charge output of the crystal was normalized by this path length, event by event. Figure 14 shows the distributions of raw charge outputs, track lengths and normalized charge outputs for three types of crystals.

We selected path-lengths of 35-100 mm for normalization. The normalization process worked well, even for KTeV and trapezoidal crystals. We obtained a clearer peak after normalization. The peak value was calculated by fitting the normalized spectrum with a Landau function. The gain constants were calculated by assuming that the energy deposited by a cosmic-ray muon per unit length in CsI is 5.63 MeV/cm, which corresponds to the energy deposited by a minimum-ionizing particle.

4-2 Calibration with punch-through muons

Another source of calibration is punch-through muons. After closing the brass shutter of 2m length in the middle of the K_L^0 beam line [13] a pure muon beam reaches the detector. It uniformly distributes over the CsI

calorimeter and is parallel to the beam axis (crystal axis). The rate of the punch-through muons at an ordinary beam of 2×10^{12}/4-sec protons on the target is a few times higher than that of cosmic rays. The trigger was made by a single cluster having a deposited energy above 40 MeV. Since the muon passes through the CsI crystal in the longitudinal direction, which is orthogonal to the cosmic-ray direction, and leaves energy of about 170 MeV, which is different from the deposited energy by cosmic rays, a calibration with punch-through muons is a good cross check of the calibration with cosmic rays.

The punch-through muon peak was seen in the raw spectrum, but became prominent by requesting no deposited energy in the neighboring crystals. In the case of the crystals at the periphery a considerable tail remained in the spectrum, as shown in Fig. 15, even after requesting a single hit. This is due to the absence of outer neighboring crystals in some directions. The gain constant was estimated from a Gaussian function fitted to the spectrum.

4-3 Comparison of the gain constants

Two gain constants obtained by cosmic rays (g_{cosmic}) and punch-through muons (g_{muon}) are compared for all crystals. A clear correlation is observed between the two constants, as shown in Fig.16.

The distribution of the ratio, $g_{\mathrm{muon}}/g_{\mathrm{cosmic}}$, is well fitted by a Gaussian function, whose mean value is 1.02 and width (σ) is 0.023. It is consistent with 1. There are several crystals apart from the Gaussian distribution. These are the crystals at the cylinder periphery, for which there remains an ambiguity in the gain constant obtained from the punch-through muons, as discussed in the previous section.

5. Calibration using 2 γ from π^0

The gain constants obtained by the cosmic-ray and punch-through muons were further refined by using the π^0 production data. For this measurement, we specially performed a run where an aluminum target with a thickness of 5 mm was placed as shown in Fig. 17. In this special run the detection system was kept at the same temperature with the same water flow in a vacuum as is the previous muon calibrations and the physics run.

For triggering we requested two clusters in the CsI calorimeter with a threshold of 100 MeV. The invariant mass of two γ's, $M_{\gamma\gamma}$, was reconstructed from their energies (E_1 and E_2) and correlation angle (θ) as

$$\mathrm{M}_{\gamma\gamma} = \sqrt{2 \cdot \mathrm{E}_1 \cdot \mathrm{E}_2 \cdot (1 - \cos\vartheta)} \,. \qquad (2)$$

The energy calibration was carried out according to the following process:

(1) We selected an event with two isolated clusters in the CsI calorimeter without any additional hit with an energy greater than 5 MeV in the barrel veto detectors.

(2) The γ energy was calculated by summing up the energies in the cluster as

$$E_\gamma = \sum_i g(i) \cdot ADC(i) \,, \qquad (3)$$

where $g(i)$ is a gain constant of the i-th crystal obtained from the energy calibration using cosmic rays.

(3) The γ incident position was at first calculated from the center-of-gravity of deposited energies in the cluster. The incident angle of γ with respect to the crystal axis was calculated by connecting the γ incident position and the target center. The real incident position was then calculated from the center of

gravity, the incident angle and a correction number from a table obtained by shower simulations.

(4) We selected γγ events of which one of the clusters had a local maximum of the deposited energy at the *i*-th crystal. If the number of these events exceeded 300 we calculated an invariant mass distribution of 2γ's. Without any correction for the gain constants the π^0 mass peak shifted from the intrinsic value of 135.0 MeV/c^2. In order to adjust the peak position all the gain constants have to be modified. But the main contributor to these events is the gain constant for the *i*-th crystal. Therefore, we calculated the correction factor ($c(i)$), as

$$c(i) = \frac{m_{\pi 0}{}^2 - (1 - R(i)) \cdot m^*_{\pi 0}(i)^2}{R(i) \cdot m^*_{\pi 0}(i)^2} \cdot \frac{< m^*_{\pi 0} >}{m_{\pi 0}}, \qquad (4)$$

where $m_{\pi 0}$ is the π^0 mass, $m^*_{\pi 0}(i)$ is the peak value of $M_{\gamma\gamma}$ for γγ combinations of the *i*-th and any other crystals, and $<m^*_{\pi 0}>$ is the mean value for all combinations obtained by the initial gain constants ($g(i)$). $R(i)$ is a mean value of the fractions of the deposited energy in the *i*-th crystal of the γ cluster. The refined gain constants are given by

$$g^C(i) = c(i) \cdot g(i). \qquad (5)$$

(5) The next process was started from $g^C(i)$ as the starting gain constant and continued until $c(i)$ converges to the unity. It was found that $c(i)$ converged after 5 iterations. Correction factors for other crystals were obtained by a similar procedure. The invariant mass distributions of 2 γ's before and after the iteration process are shown in Fig. 18.

The correction factors from the initial to the final gain constants distribute as shown in Fig. 19. The gain constants for about 40% of the crystals were not refined by this process because they were located at the

periphery of the calorimeter, and/or because of poor statistics. The gain constants for 60% of the crystals were systematically shifted by 7% from the initial values obtained by the cosmic-ray calibration. The width of this distribution was 3% in σ. It should be mentioned that the gain constants refined by this method include the effect of the shower leakage from the rear of the CsI crystal. The shower leakage from the rear of the crystal was calculated to be about 3% for the main CsI. We are studying about the remaining 4 %. The effect with muons spectra might be a cause of it.

Table 1 gives the mass and width obtained from the π^0 and η peaks for four sets of gain constants:

(1) All CsI crystals were used with the initial set of gain constants (see Fig.18(a)).
(2) 60% of CsI crystals were used with the corrected gain constants (see Fig.18(b)).
(3) All CsI crystals were used, of which gain constants of 60% were corrected but those of 40% were the initial values.
(4) All CsI crystals were used, of which gain constants of 60% were corrected and those of 40% were shifted by 7%.

In the second case, by the gain correction, the masses of π^0 and η are well reproduced and the widths are significantly narrowed. The third case shows a slightly worse result, but the fourth case shows almost the same result as the second case. Then we use the gain constants of the fourth case.

6. Timing calibration with cosmic rays

6.1 Timing calibration

We performed an in-situ timing calibration of the CsI calorimeter using cosmic rays. The signal propagated as shown in Fig. 20.

The hit timing ($T(i,j)$) of the i-th CsI crystal in the j-th cosmic-ray event was obtained by converting the TDC value using a conversion factor for each i-th channel, which was calibrated by a standard pulser. The $T(i,j)$ can be written as

$$T(i,j) = a(i) + b(i) + cf(i,j) + cz(i,j) - T_0(i,j), \qquad (6)$$

where

$a(i)$: propagation time from the photo-cathode of PMT to the input of the Amp-Disc module. However, in the later analysis, $a(i)$ is redefined as $a(i) - \langle a(i) \rangle$, where $\langle a(i) \rangle$ is an average value of $a(i)$ over all crystals and it is included in $T_0(i,j)$ as a constant term.

b (i): signal propagation time from the input of the Amp-Disc module to TDC. We used the value measured by employing the pulser for every channel.

$cf(i,j)$: correction factor for the flight time of cosmic rays among CsI modules. Using a reconstructed track we calculated the intersection point and track length. The velocity of the cosmic ray was assumed to be 30cm/ns.

$cz(i,j)$: correction factor for the travel time of the scintillation signal in the CsI module. For the cosmic-ray track inclined with respect to the CsI calorimeter plane we can know the entrance and exit points of cosmic rays and then estimate the intersection of the track with the crystal in the z-direction.

$T_0(i,j)$: trigger (TDC-start) timing for the j-th event. It can be estimated from Eq.(6) for every i-th hit crystal, but $T_0(i,j)$ should be the

same for all hit crystals.

Among them, $T(i,j)$, $b(i)$, $cf(i,j)$ and $cz(i,j)$ are given by the measured data, and the goal of the calibration is to obtain the values of $a(i)$ under a constraint that $T_0(i,j)$ are the same for all hit crystals. Then $a(i)$ was corrected as $a(i) = a(i) + \Delta(i)$, using

$$\Delta(i) = T_0(i,j) - \langle T_0(i,j) \rangle , \qquad (7)$$

where $\langle T_0(i,j) \rangle$ is an averaged value over i of $T_0(i,j)$. Actually, the correction was redundantly carried out in the following steps.

In the first step, we made the flight-time correction, ($cf(i,j)$), and assumed $a(i)$ and $cz(i,j)$ to be zero. $\Delta(i)$ of Eq.(7) was calculated and $a(i)$ was corrected. The mean values were used as the starting parameters of the next step.

In the second step, we introduced the $cz(i,j)$ correction. In this step we analyzed only the events in which the z-position could be calculated from the trajectory. This was the case when cosmic ray crossed the CsI wall inclined in the z direction, and the track was fully contained in the CsI calorimeter, as shown in Fig. 21. The crystals at both ends of the track correspond to the entrance and exit of the cosmic ray.

For these tracks we first calculated the timing difference between these end crystals using $a(i)$ corrected in the second step. Two clear peaks, which correspond to the cosmic-ray incidence at the front or back face, are seen in the distribution of the timing difference, as shown in Fig. 22(a). The peak positions deviate by $\pm$3.3ns from zero. This deviation corresponds to the propagation time of light for 30 cm in CsI and we obtained an effective light speed of 9.1 cm/ns. After making the $cz(i,j)$ correction using this effective light speed, two peaks merged into one peak with a resolution of 1 ns, as shown in Fig. 22(b).

cz corrections for the peripheral crystals were also made by using the

z track position derived from the fit of the timings of the inner crystals.

In the third step we made a time slew correction using the ADC data. A scatter plot of the timing and the signal charge is shown in Fig. 23. By fitting these data we obtained the time slew correction function as $\Delta t_{\mathrm{walk}}(\mathrm{ns}) = 5.5/(Q(\mathrm{pC}))^{1/2}$.

The distribution of the time difference between any pair of crystals in a cosmic-ray track is shown in Fig. 24 at each correction step. An improvement of the timing resolution in every step is clearly seen and, after the time slew correction, the width of the distribution is 0.8 ns in σ.

6-2 Trimming of cables for triggering

During the calibration we adjusted the timing at the input of the Amp-Discri modules. Figure 25 is a plot of $a(i)$ vs the applied high voltage(HV) to each PMT. As shown in Fig. 25(a), a correlation is clearly observed between $a(i)$ and the HV and three groups of points that correspond to the type of PMT's used for three types of crystals. We trimmed the cable length of $a(i)$ and adjusted the signal mixture for the trigger within ± 2 ns, as shown in Fig.25(b).

7. Mass and Timing Resolution for $K_L^0 \rightarrow \pi^0\pi^0\pi^0$ events

In the physics run we simultaneously collected the data of $K_L^0 \rightarrow \pi^0\pi^0\pi^0$ decays and reconstructed the K_L^0 mass using the 6γ events detected by the CsI calorimeter as an overall check of the energy and timing calibration.

First, we selected an event with 6 isolated γ's. From these γ's we calculated for all combinations of two gammas the vertex point of an assumed $\pi^0 \rightarrow \gamma\gamma$ decay using the π^0 mass. At first the γ hit position was calculated from the center of gravity of the energy distribution in each cluster. After obtaining the π^0 vertex position and the incident angle of γ to the CsI wall, the γ hit position was recalculated using the angle-correction table, which was mentioned in Item (3) of Section 5.

There are 15 combinations of γ to reconstruct $3\pi^0$ events. We selected the combination which has the minimum spread among three reconstructed $\pi^0 \rightarrow \gamma\gamma$ vertex points.

The $3\pi^0$ invariant mass distribution is shown in Fig. 26. A clean peak can be observed at the K_L^0 mass with very small backgrounds. The mass width is 4.3 MeV in σ.

For these $K_L^0 \rightarrow \pi^0\pi^0\pi^0$ events we calculated the difference of the hit timing of 6 individual γ's from the average by using the calibration constant obtained from the cosmic-ray measurement. In this case the γ hit timing was defined as the hit timing of the CsI with the local energy maximum in the γ cluster. The time of flight difference and the time slew were corrected. The result is shown in Fig. 27, where the resolution is 0.51 ns in σ.

7. Summary and Discussion

The electromagnetic calorimeter consisting of 576 undoped CsI crystals was used in the KEK-PS $K_L^0 \rightarrow \pi^0 \nu \bar{\nu}$ experiment (E391a). The crystals were mounted in a support cylinder with a diameter of 2 m and contained in a vacuum vessel. We made an in situ calibration of their gains using cosmic-rays and punch-through muons at the K_L^0 beam area. Two gain constants obtained by both methods differ by only 2% and the ratio has a narrow distribution with of a σ of 2.3%. The hit timing of each crystal was also calibrated by using cosmic rays. The absolute values of the gain constants were further calibrated using π^0's produced by neutron interactions.

Using these calibration constants we reconstructed $K_L^0 \rightarrow \pi^0\pi^0\pi^0$ decays and obtained a K_L^0 mass resolution of σ=4.3 MeV/c^2 and a timing resolution of 0.51 ns.

Since a large number of $K_L^0 \rightarrow \pi^0\pi^0\pi^0$ decay samples were collected during the physics run we can use these data for the re-calibration of the CsI calorimeter in order to refine the resolutions further. The details of the re-calibration will be reported later.

Acknowledgements

The authors express their sincere thanks to the operating staff of the 12-GeV KEK proton synchrotron and the beam channel group for providing us a good quality neutral beam to the E391a detector. This work has been partly supported by a Grant-in-Aid from the Ministry of Education, Culture, Sports, Science and Technology in Japan and by the Japan Society for the Promotion of Science (JSPS). One of us (M.D.) acknowledges the receipt of the Japanese Government Scholarship (Monbukagakusho; MEXT) during this work.

References

[1] T. Inagaki, *et al.*, "Measurement of the $K_L^0 \rightarrow \pi^0 \nu\bar{\nu}$", Proposal of an experiment at the KEK 12-GeV proton synchrotron, KEK Internal 96-13, Nov.1996, H.

[2] G. Buchara and A. J. Buras, Phys.Rev. **D**54 (1996) 6782.

[3] A. Alavi-Harati, *et al.*, Phys. Rev. **D**61 (2000) 072006.

[4] J-PARC, http://j-parc.jp.

[5] E. Frlez, *et al.*, Nucl. Instr. And Meth. **A**526 (2004) 300.

[6] Borrowed from the KTeV group, Fermilab. R. S. Kessler *et al.*, Nucl. Instr. and Meth. **A368** (1996) 653.

[7] Previously used in the KEK-PS E162 experiment. T. Nomura *et al.*, Phys. Lett. **B408** (1997) 445.

[8] METACAST 5448, MERECO Technologies, West Warwick, R.I. 02893, USA.

[9] Y. Sugaya, *et al.*, "DAQ system for the $K_L^0 \rightarrow \pi^0 \nu\bar{\nu}$ search at KEK-PS" 13th IEEE NPSS Real Time Conference, Conference Records RT-034 (2003).

[10] LeCroy 1885F, LeCroy Research Systems Corp., Chestnut Ridge, NY. USA.

[11] O. Sasaki, et al., IEEE Trans. Nucl. Sci. **vol 35**, pp.342-345, 1988.

[12] S. Ritt and P. A. Amaudruz, " The MIDAS DAQ system" (2002). Available from http://midas.triumf.ca.

[13] H. Watanabe, Doctor Thesis, 2002, Graduate School of Science and Engineering, Saga Univ., Saga, Japan.

]

Table 1 Mass and width of π^0 and η peaks obtained by four sets of gain constants. Cases (1)-(4) are described in the text.

	(1)	(2)	(3)	(4)
π^0 Mass [MeV/c^2]	126	135	134	135
Width(σ)	4.8	4.3	5.0	4.6
η Mass [MeV/c^2]	508	548	545	548
Width(σ)	19.1	13.5	14.8	14.1

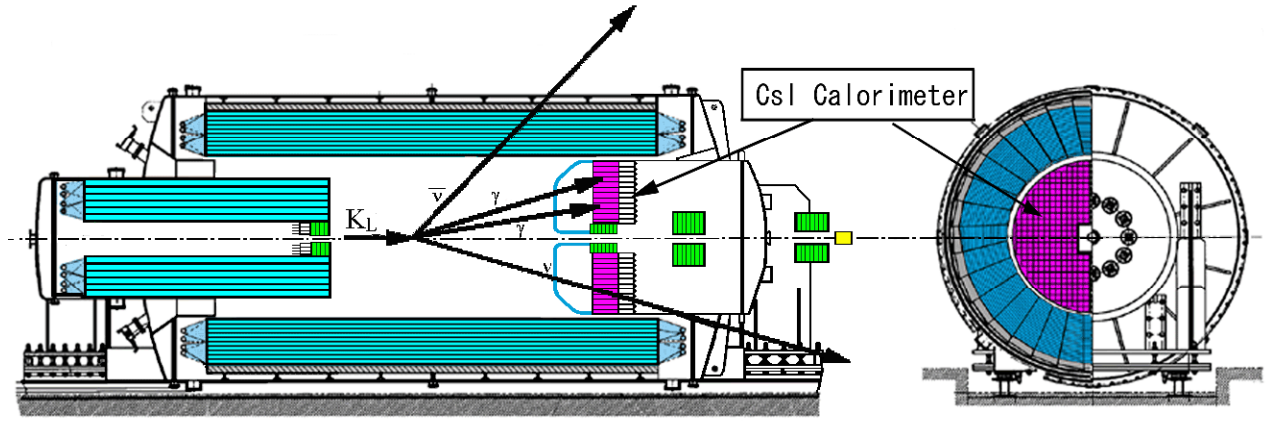

Fig.1: E391a detector. A CsI calorimeter with a disc shape and a diameter of 2 m is placed downstream of the detector. Cylindrical photon veto detectors made of lead-scintillator sandwiches surround the K_L^0 decay region and the CsI calorimeter. All of these detectors are placed in a cylindrical vacuum vessel with a diameter of 3.8 m and a length of 8.7 m.

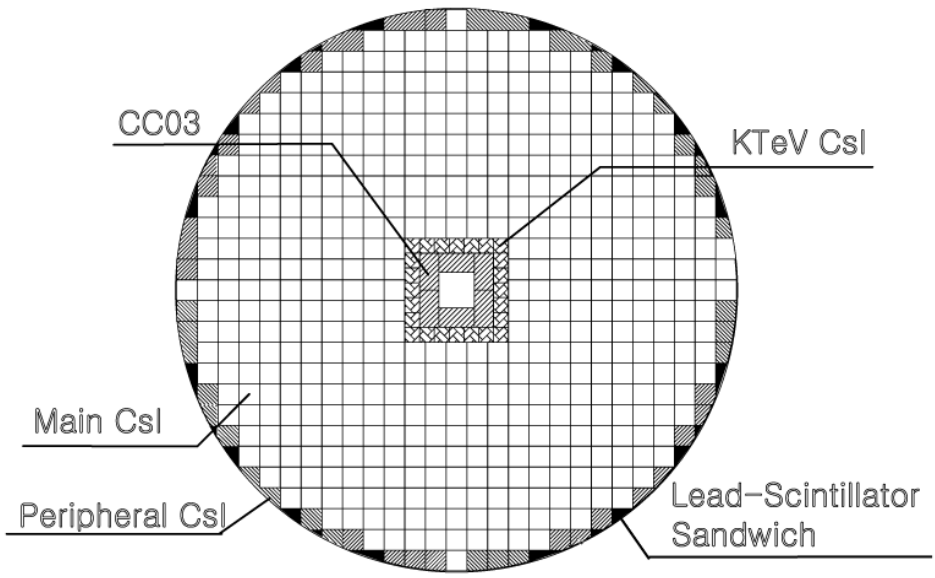

Fig.2: Arrangement of CsI crystals.

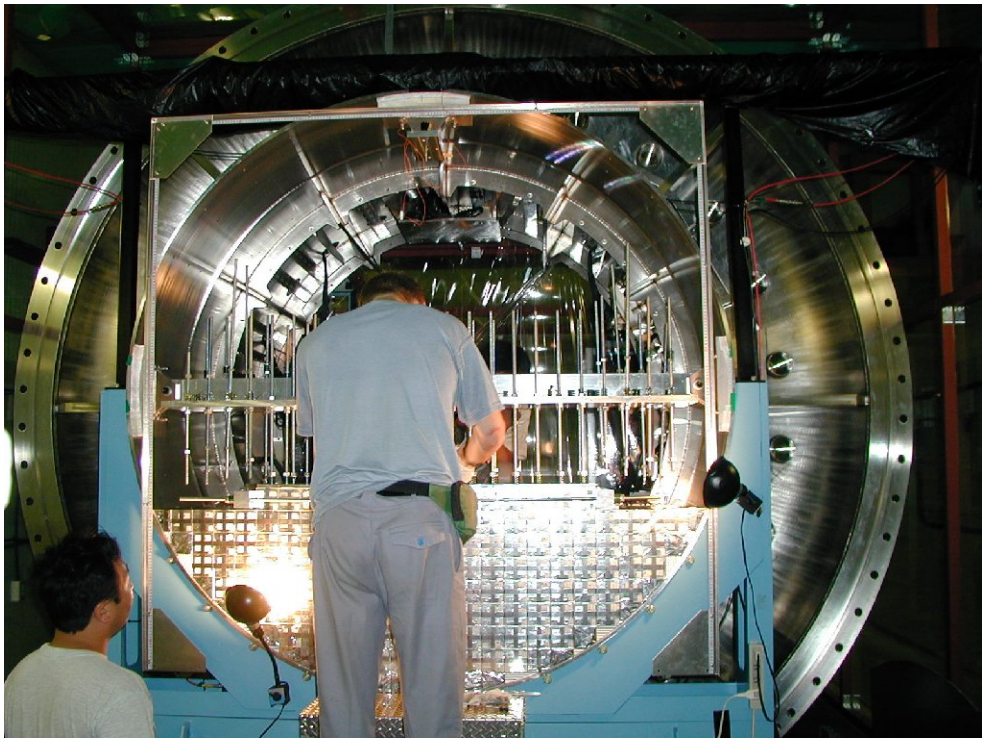

Fig.3: Stacking process.

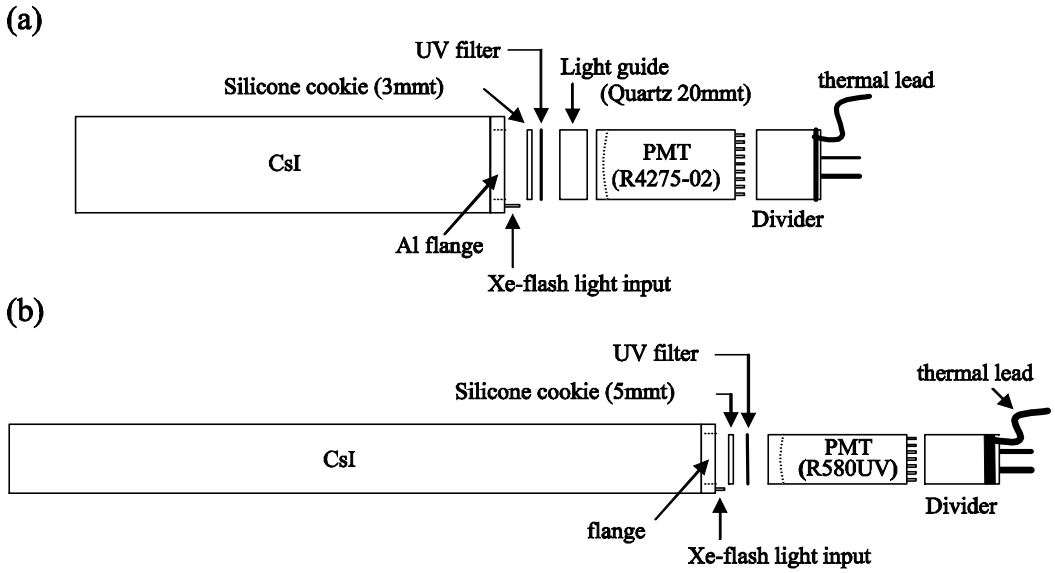

Fig.4: Schematic drawings of the CsI modules. (a) The Main CsI ($70x70x300mm^3$) and (b) The KTeV CsI ($50x50x500mm^3$).

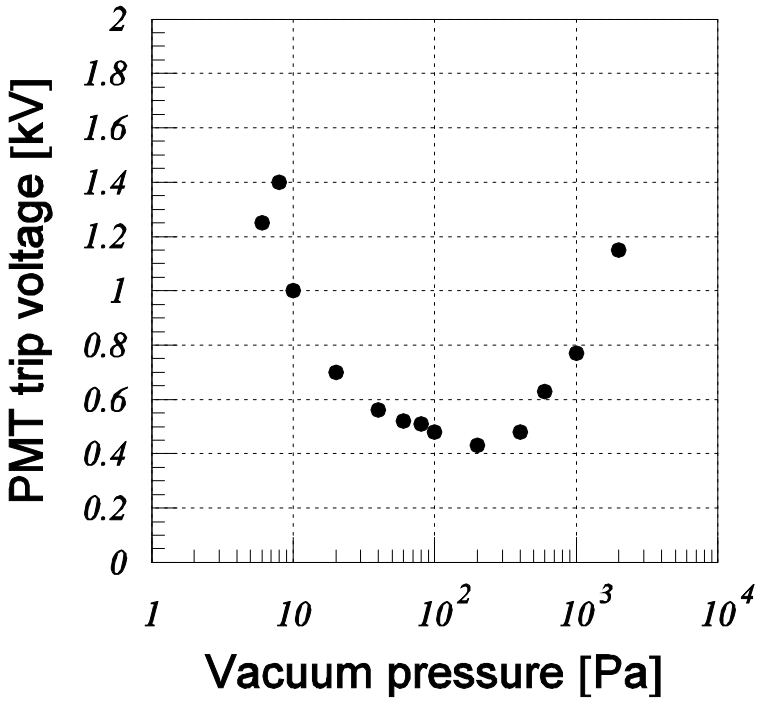

Fig.5: PMT trip voltage vs. vacuum pressure.

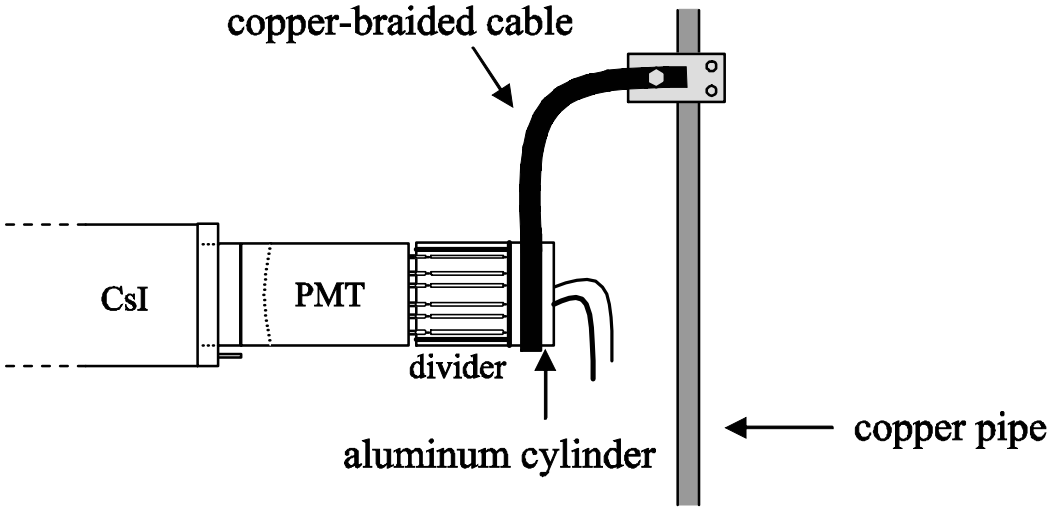

Fig.6: Cooling scheme of the PMT divider. Thermal connection between the PMT divider and the cooling pipe is made by a copper-braided cable.

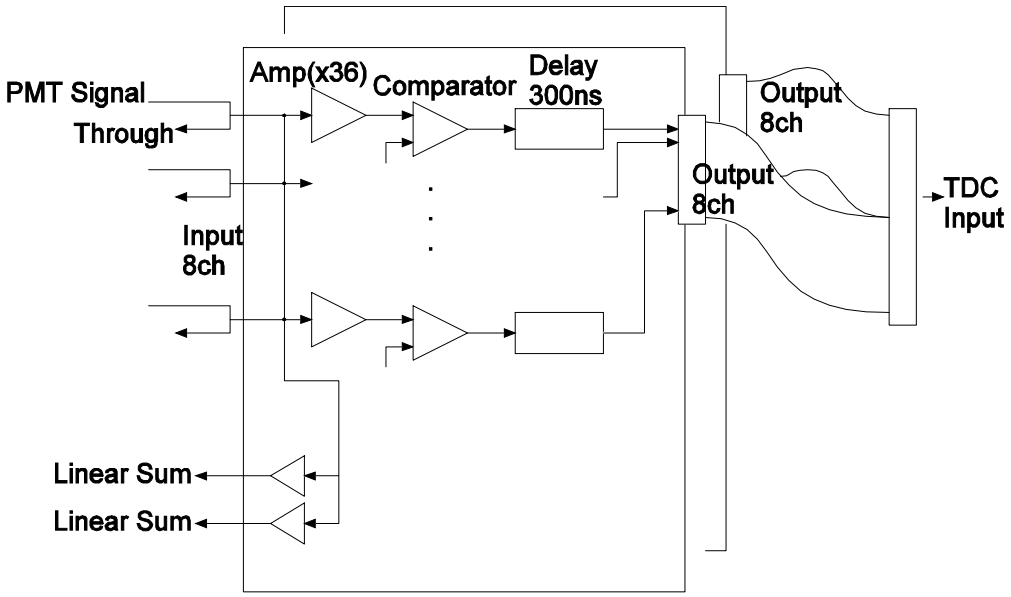

Fig.7: Diagram of the Amp-Discri module.

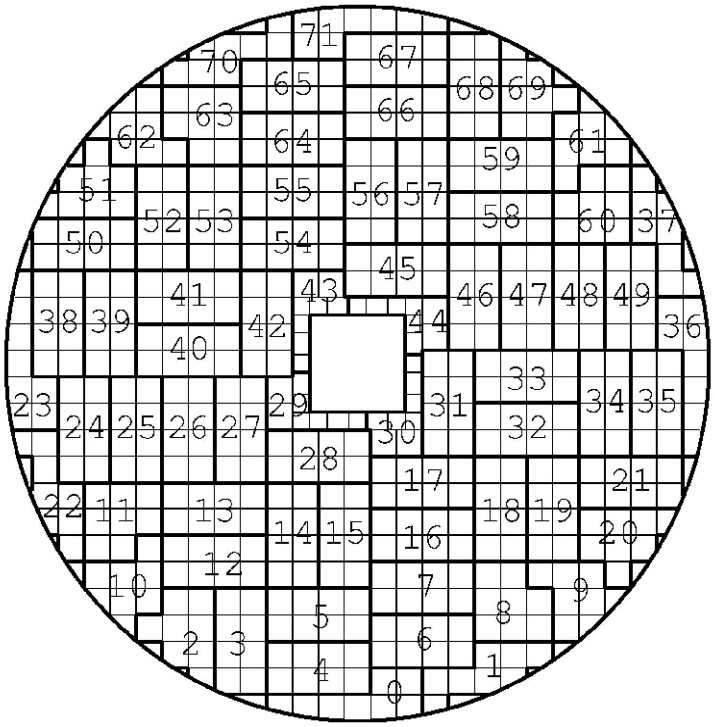

Fig. 8: Pattern to bundle eight CsI blocks for a sum signal.
In total, 72 clusters are formed for event triggering.

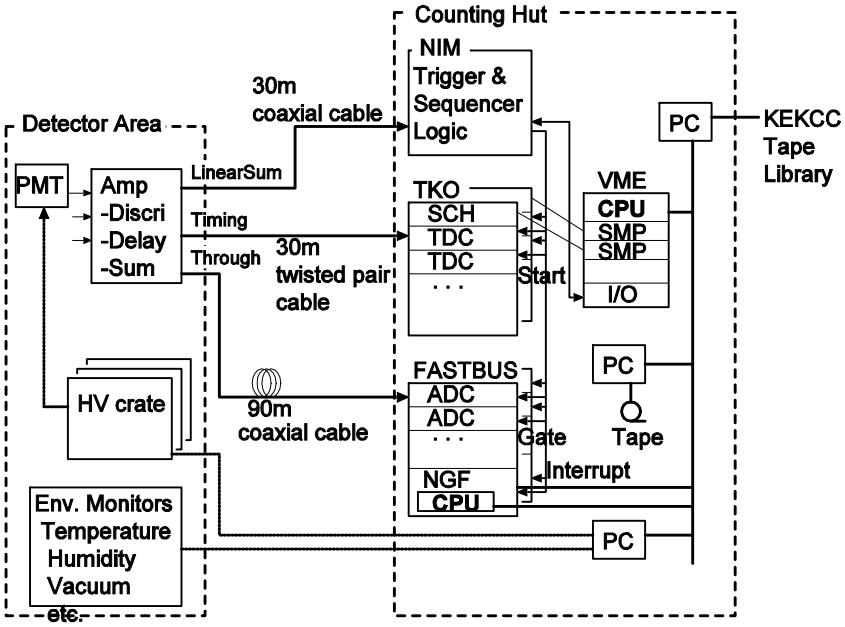

Fig.9: DAQ system of the E391a experiment.

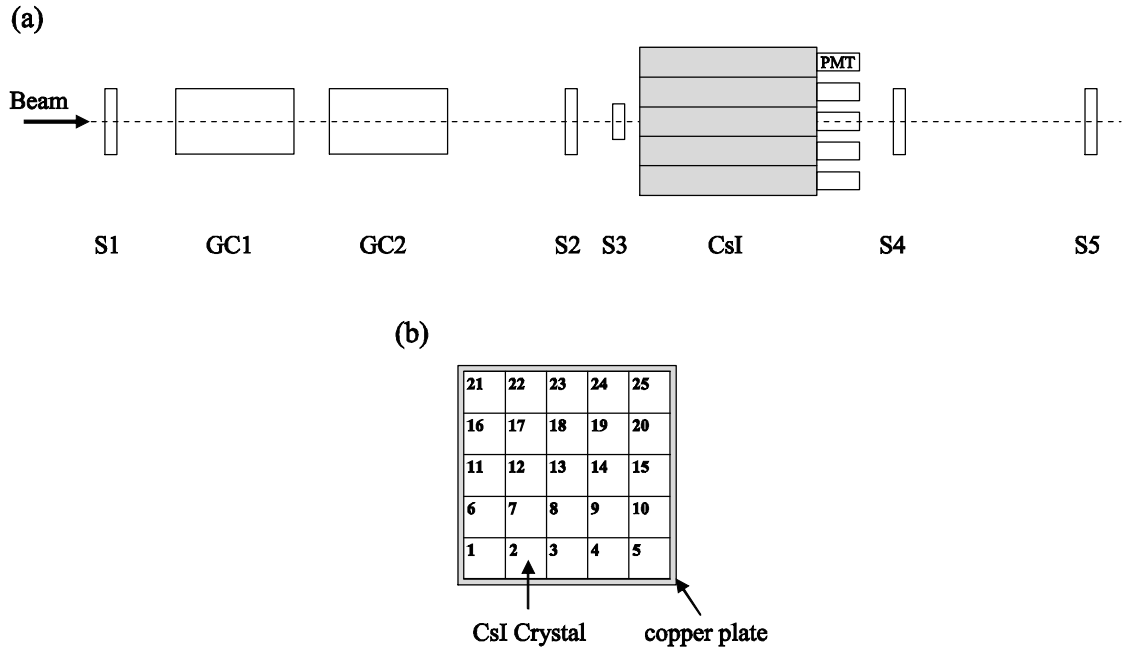

Fig. 10: Setup for the test-beam experiment at the KEK 12-GeV proton synchrotron. (a) Beam trigger counters. S1-S5: plastic scintillation counters, GC1 and GC2: gas Cherenkov counters. (b) Front view of 25 crystals stacked in a 5 x 5 matrix.

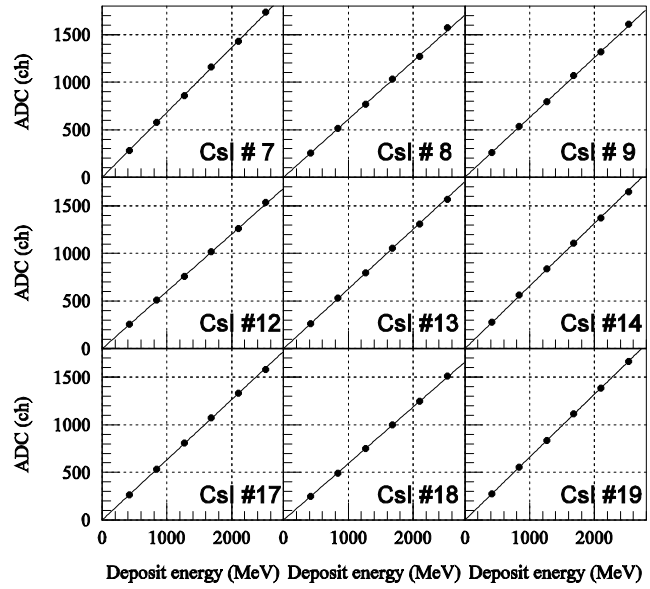

Fig.11: Relation between the energy deposit and the ADC peak positions for 9 crystals. The lines are the linear fits of the experimental data.

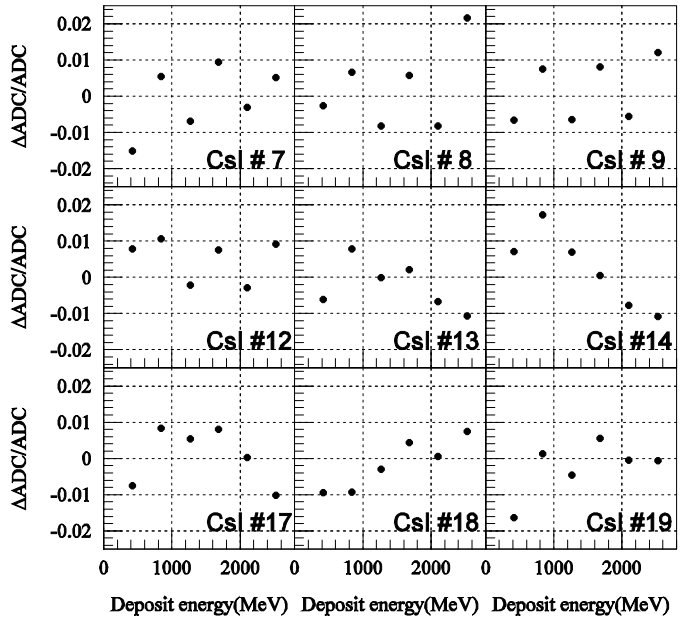

Fig.12: Discrepancies between the experimental data and the linear fits for 9 crystals.

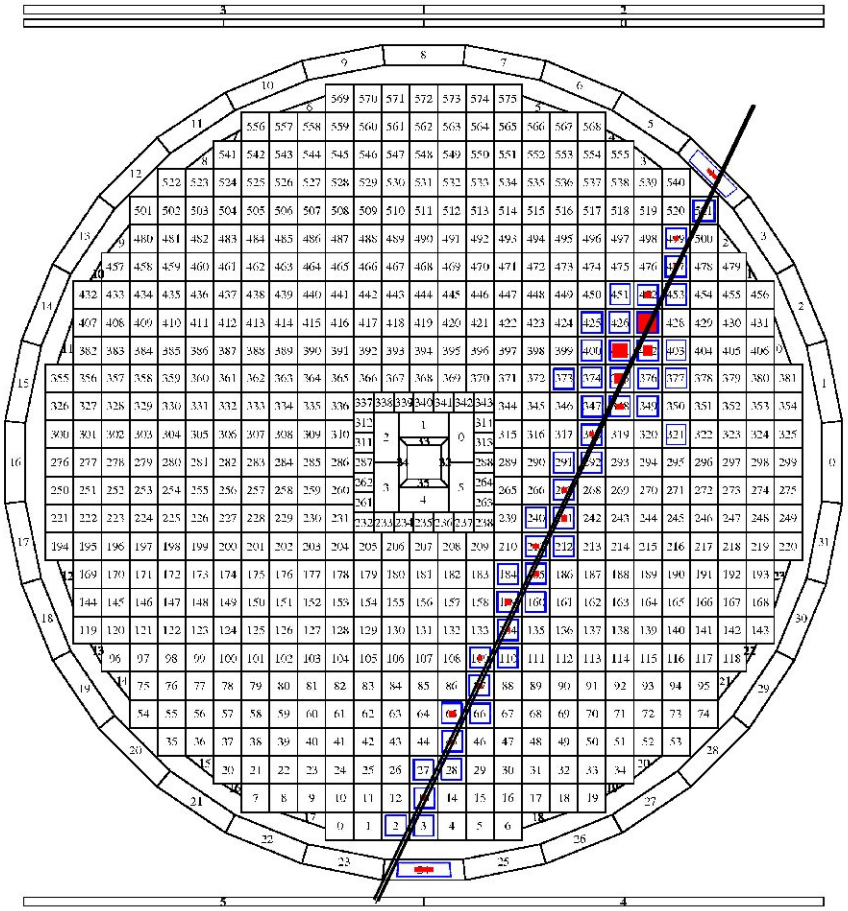

Fig.13: Typical cosmic-ray track. The open square and the size of the shaded square in the CsI crystal indicate TDC signal and the amount of the presence of deposited energy. The line is a linear fit to the hit crystals.

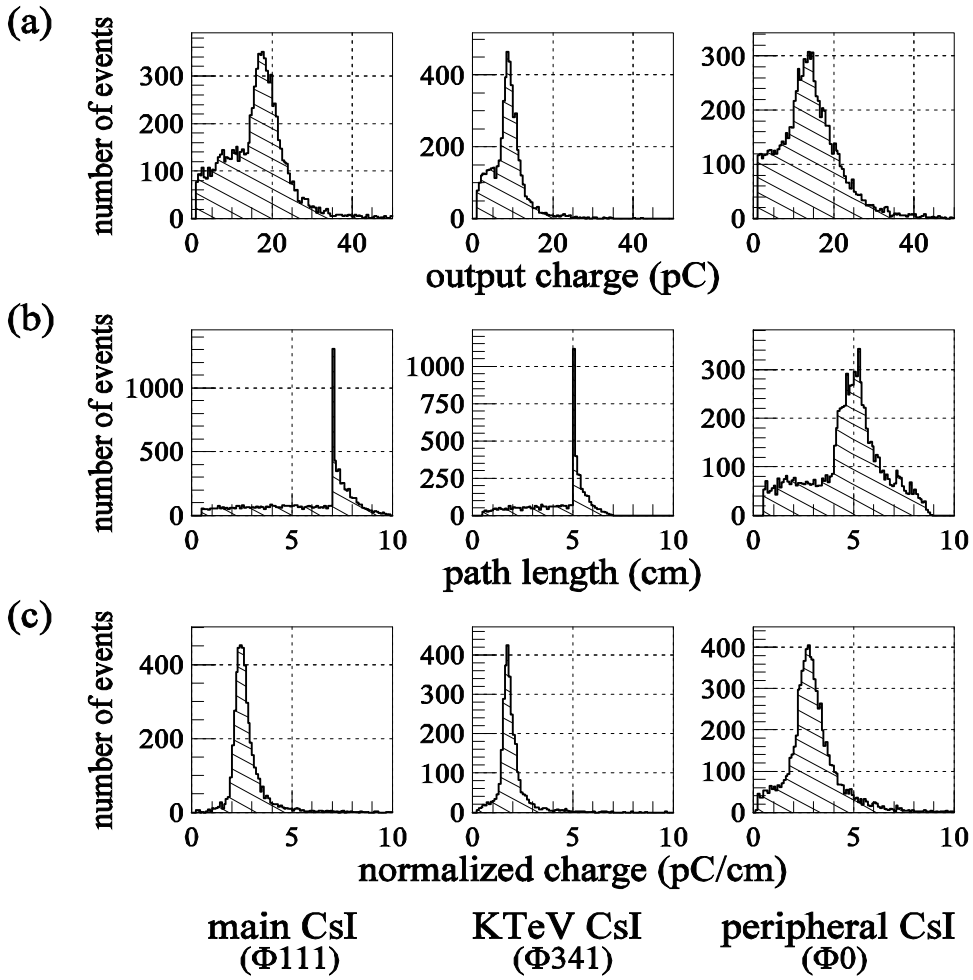

Fig. 14: (a) Raw charges, (b) path-lengths and (c) normalized-charges for three types of crystals, main CsI(#111), KTeV CsI(#341) and peripheral CsI (#0) with a trapezoidal shape.

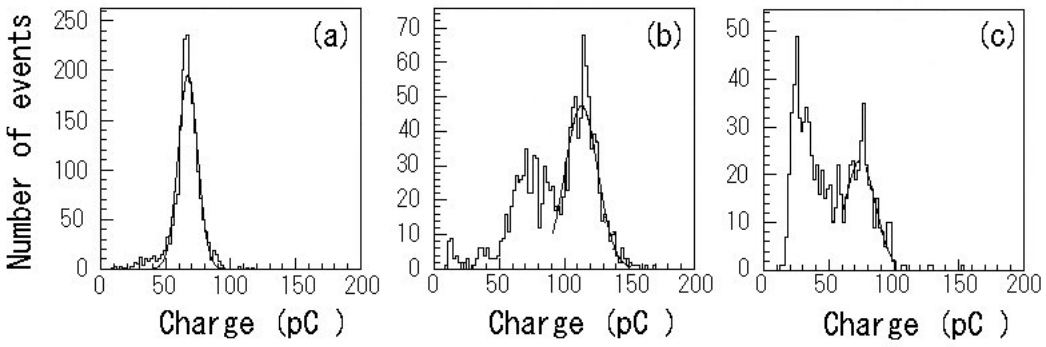

Fig.15: Charge spectra for punch-through muons for three types of crystals: (a) the Main CsI, (b) the KTeV CsI and (c) the trapezoidal CsI crystals. The curves are fits with Gaussian functions.

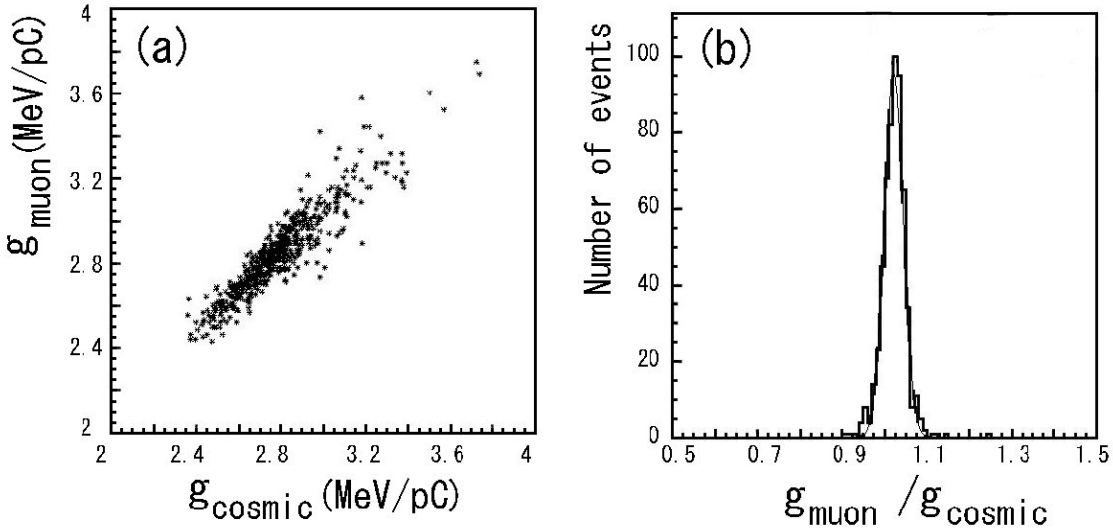

Fig.16: Comparison of gain constants obtained by cosmic-ray and punch-through muons. (a) Scatter plot and (b) distribution of the ratio, g_{muon}/g_{cosmic}.

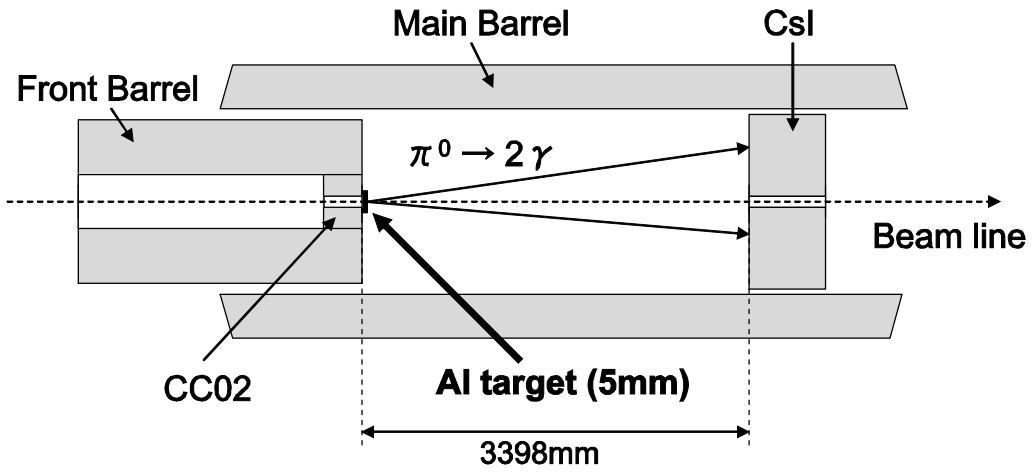

Fig.17: Setup for the measurement of π^0's produced from an aluminum target hit by neutrons.

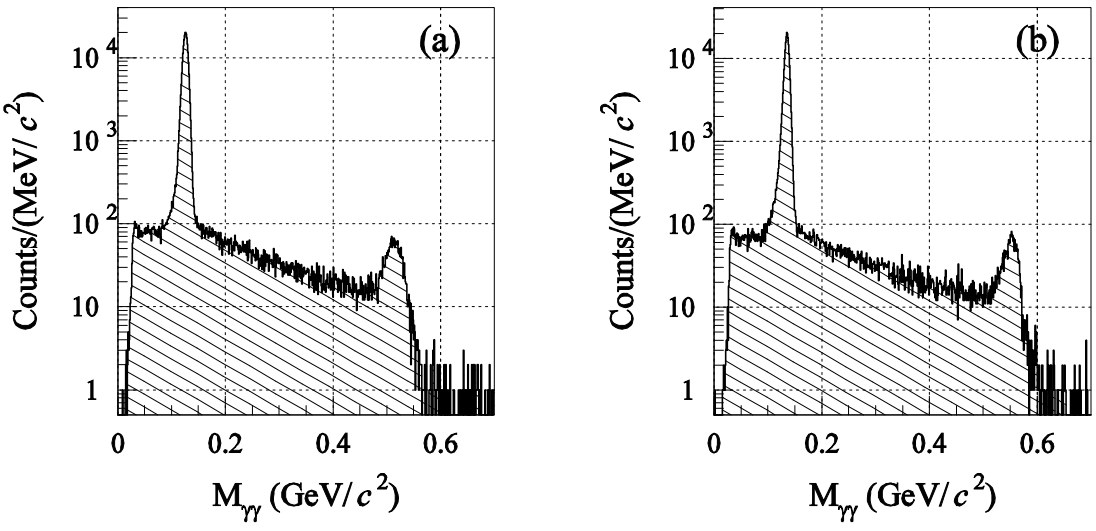

Fig.18: Invariant mass spectrum of 2γ's from the aluminum target hit by neutrons; (a) before iteration, (b) after 5 iterations.

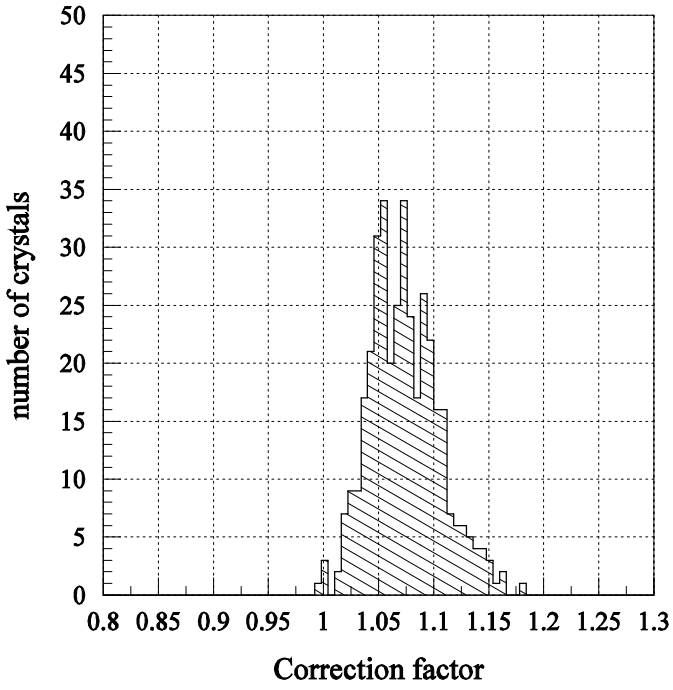

Fig.19: Correction factors obtained by the CsI calibration with π^0's.

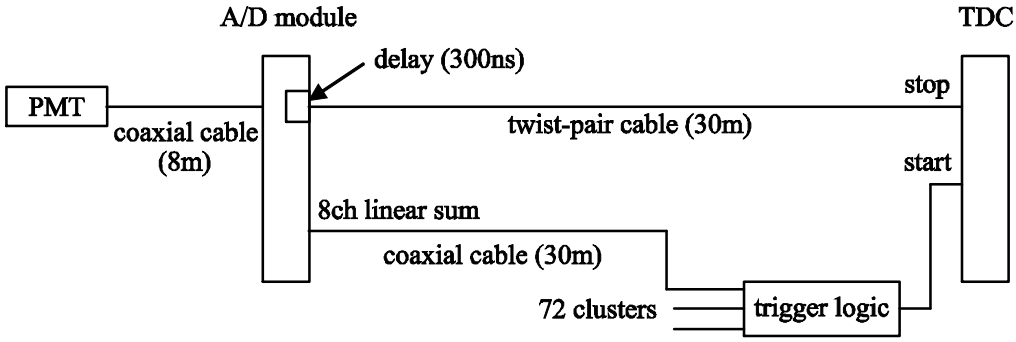

Fig.20: Scheme of signal propagation from PMT to TDC.

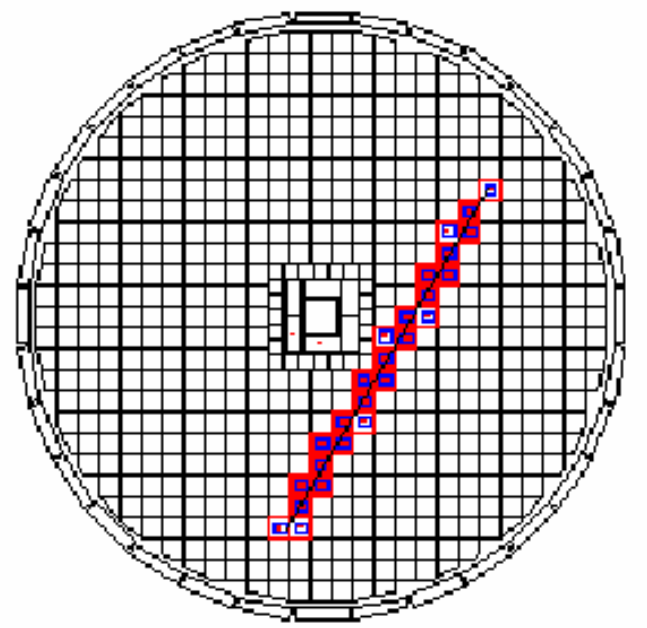

Fig.21: Example of a cosmic-ray track which crossed the CsI wall.

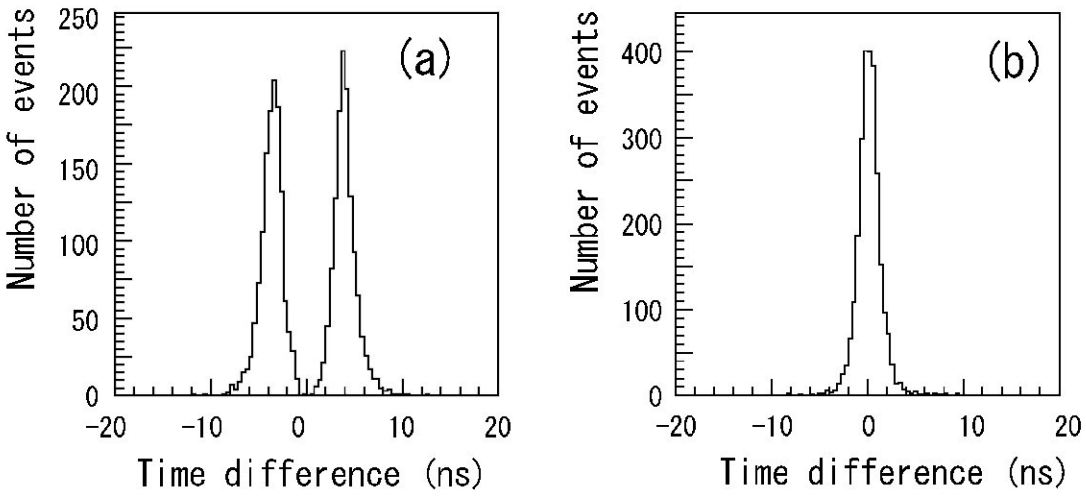

Fig.22: Hit timing difference between two crystals; the entrance and exit crystals. (a) Before the *cz* correction, and (b) after the *cz* correction.

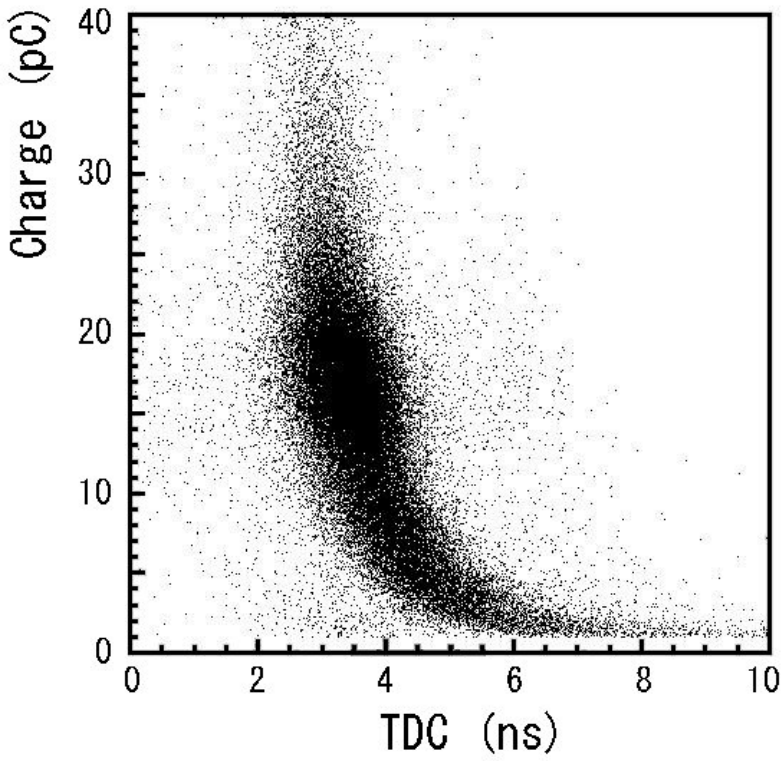

Fig.23: Scatter plot of the hit timing and the signal charge for cosmic-ray tracks.

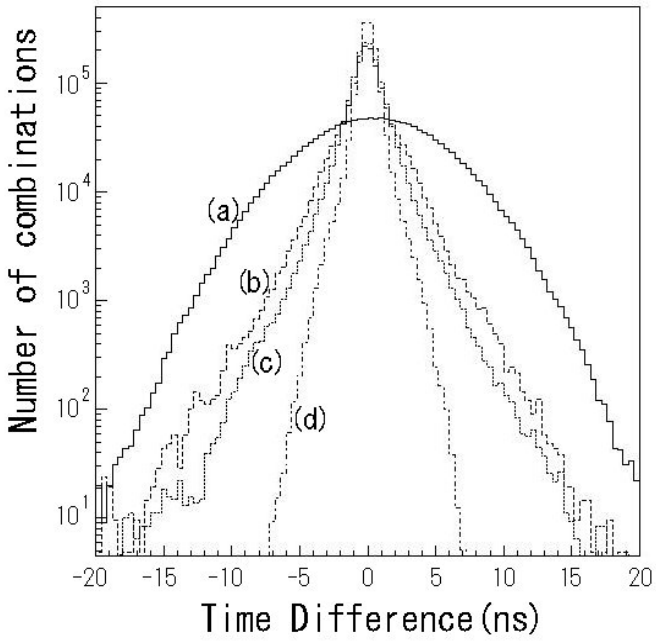

Fig.24: Distribution of the time difference between any two crystals in a track after each step of corrections. (a) Before *a(i)* calibration with the cosmic ray time of flight correction (*cf*-correction), (b) after *a(i)* calibration, (c) after a z-position correction (*cz*-correction) and (d) after a time slew correction.

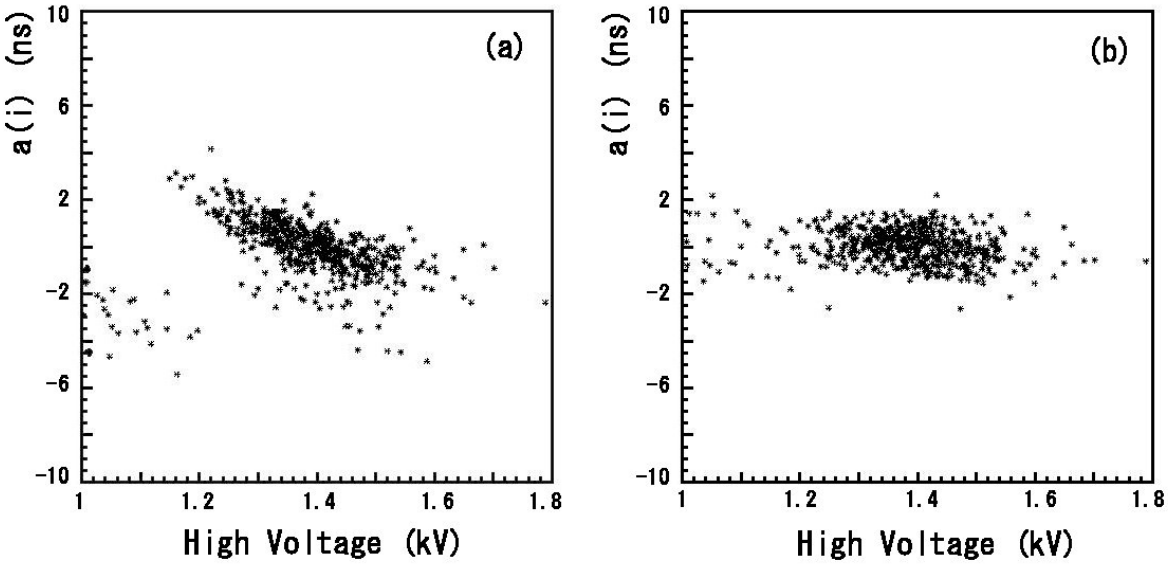

Fig.25: Correlation between *a*(*i*) and PMT-HV's. (a) Before and (b) after cable trimming.

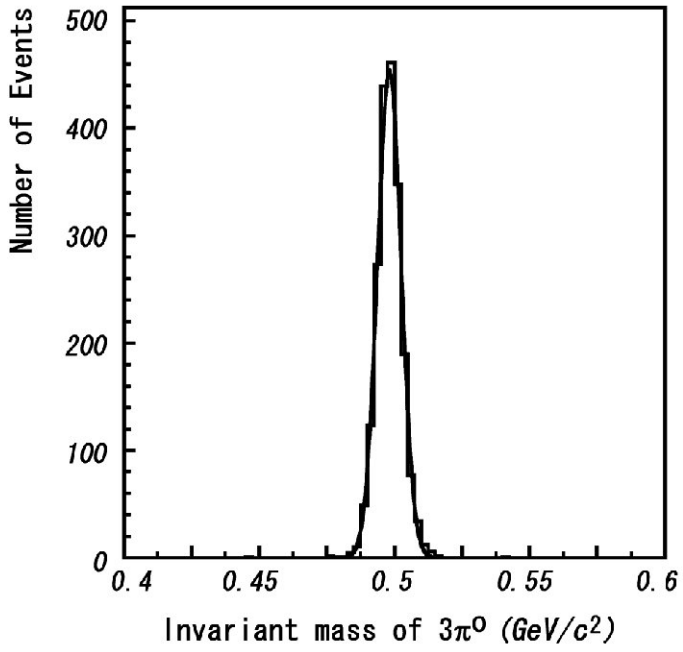

Fig.26: Invariant mass spectrum of $3\pi^0$ from the K_L^0 decays.

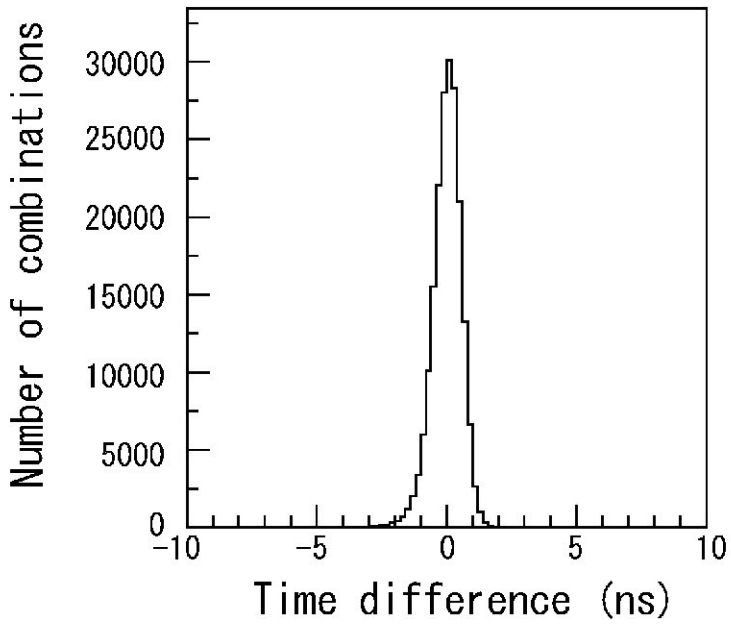

Fig.27: Time-difference distribution among 6 γ's for $K_L^0 \rightarrow \pi^0\pi^0\pi^0$.